Bol. Soc. Paran. Mat.
©SPM – E-ISSN-2175-1188
SPM: www.spm.uem.br/bspm

(3s.) **v. 2026 (44) 4** : 1–24.
ISSN-0037-8712
doi:10.5269/bspm.80318

Entropy Generation on Magneto Rotating Flow of Hybrid Nanofluid with Porous Medium in the Presence of Darcy Dissipation

Mandya Seenaiah Pooja, Joghaylla Santhosh Kumar, Kammasandra Munivenkataswamy Praveena Kumara and Sibyala Vijayakumar Varma

ABSTRACT: The recent study in nanofluid applications has significantly advanced thermal transport technologies, especially with the emergence of hybrid nanofluids, engineered by dispersing distinct nanoparticles into conventional base fluids. These hybrid formulations provide synergistic thermal enhancements due to their improved thermophysical behavior. In this theoretical investigation, the magnetohydrodynamic (MHD) flow of a viscous hybrid nanofluid is examined within a rotating porous medium confined between parallel plates. The flow system incorporates effects such as Joule heating, thermal radiation, heat generation/absorption, chemical reaction with Arrhenius activation energy, and Darcy dissipation. Both velocity and thermal slip boundary conditions are considered. Entropy generation analysis is also included to assess system irreversibility. The governing nonlinear equations are solved numerically using the bvp4c solver in MATLAB. The study explores the influence of governing parameters on velocity, temperature, concentration, skin friction, Nusselt number, and entropy generation rate. Results reveal that the rotation and magnetic parameters significantly affect the velocity field. At the same time, thermal characteristics are sensitive to the Prandtl number, Eckert number, and Darcy effects within the porous structure.

Keywords: Darcy dissipation, MHD, parallel plates, entropy analysis, thermal radiation, activation energy.

Contents

2020 *Mathematics Subject Classification:* 76W05, 76D05, 76S05, 76R10, 80A20, 80A17, 35Q30.
Submitted November 23, 2025. Published February 26, 2026

1. Introduction

Hybrid nanofluids, consisting of a mixture of two or more types of nanoparticles suspended in a base fluid, have emerged as advanced working fluids due to their superior thermal properties. These fluids typically incorporate various nanoparticles such as metals, metal oxides, or carbon-based materials, which enhance thermal conductivity, viscosity, and heat capacity. Their enhanced thermophysical characteristics make them highly suitable for applications in thermal management systems, including heat exchangers, electronic cooling devices, and energy storage systems. Numerous studies have been conducted to understand their heat transfer performance and rheological behaviour. Magnetohydrodynamic (MHD) effects have been widely analyzed due to their importance in nuclear reactors, cooling technologies, and metallurgical processes. Researchers have investigated different physical aspects such as magnetic fields, viscous dissipation, porous media, chemical reactions, and variable thermal conductivity to understand how irreversibilities affect heat and mass transfer. The following review summarizes the most relevant contributions in this area. In their work, Abbas et al. [1] analyzed entropy generation in MHD viscous fluid flow through a vertical porous channel under thermal radiation. They observed that magnetic fields and viscous dissipation strongly influence flow irreversibility, with entropy generation increasing under stronger thermal effects. Similarly, Abdelhameed [2] examined mixed convection nanofluid flow with chemical reactions and highlighted how nanoparticle concentration affects thermal transport and entropy minimization strategies. Al-Odat et al. [3] studied laminar forced convection with a magnetic field at a flat plate and reported that magnetic forces intensify entropy generation while altering thermal boundary layer characteristics. Awad [4] provided a broad review of entropy generation in microchannels and concluded that microscale effects and geometrical configurations play a critical role in enhancing or reducing irreversibility.

Further studies have emphasized geometric influences on entropy generation. Bahaidarah [5] explored sharp-edged wavy channels and found that flow disturbance increases entropy production, making geometry a key design factor. Along similar lines, Balamurugan et al. [6] analyzed Couette flow with aligned magnetic fields and radiation, showing that dissipative effects dominate entropy generation under strong thermal gradients. The role of Joule heating was stressed by Chakraborty et al. [7], who demonstrated that narrow channels under electromagnetic fields experience significant increases in entropy due to viscous dissipation. Earlier, Chamkha [8] and Cox [9] provided foundational work on immiscible and porous channel flows, laying the groundwork for entropy analysis in multiphase and porous systems. Building on these foundations, Das et al. [10] focused on hybrid nanofluids and showed that adding metallic nanoparticles enhances heat transfer but also contributes to higher entropy generation.

Entropy generation in unsteady and rotating flows has also been investigated. Dawar et al. [11] studied MHD squeezing flow of carbon nanofluids in rotating channels and found that viscous dissipation amplifies entropy generation, especially in transient regimes. Dogonchi et al. [12] further expanded this to two parallel disks with radiation and different nanoparticles, revealing that nanoparticle type significantly alters entropy behavior. Ebrahimi et al. [13]explored microchannels with longitudinal vortex generators and highlighted their potential for improving thermal performance despite entropy penalties. Eid and Nafe [14] investigated hybrid nanofluids with slip effects in porous media and noted that entropy generation depends strongly on thermal conductivity variations. More recently, Enamul et al. [15,16] presented detailed analyses of Darcy-Forchheimer hybrid nanofluids bounded by disks, showing that Hall currents and thermal conductivity variations influence entropy production in coupled-rotating systems.

Several researchers have emphasized magnetohydrodynamic and radiation-driven flows. Hayat et al. [17] and [18] examined rotating disks and highlighted the role of Lorentz forces, viscous dissipation, and Joule heating in entropy generation. Hooman. [19] focused on microscale convection and found that slip boundary conditions, temperature jumps, and dust presence alter irreversibility. Ibáñez et al. [20] studied slip flow in parallel plate microchannels and showed that nonlinear thermal radiation significantly enhances entropy. Khan et al. [21,22,23,24] analyzed entropy in hybrid nanofluid systems, including cubic autocatalytic squeezing flows and triple diffusive convection, concluding that chemical and porous effects amplify irreversibility. Kiyasatfar [25]studied power-law fluids and found that entropy increases under strong viscous dissipation in microchannels.

Other studies explored turbulence, nonlinear radiation, and hybrid effects. Lopez et al. [26] and Mahian et al. [27] reviewed entropy in MHD nanofluids, concluding that nonlinear effects and nanoparticle

concentration control entropy trends. Makinde [28] analyzed vertical porous plates under free convection and reported strong irreversibility due to radiation. Manay et al. [29] studied microchannel sinks and showed that entropy is sensitive to geometric constraints. Murshid et al. [30] investigated rotating hybrid nanofluid plates with activation energy, while Murugan et al. [31] emphasized the combined influence of thermo-radiation and ohmic dissipation. The classical work of Ordóñez and Bejan [32] provided optimization strategies for counterflow heat exchangers through entropy minimization, forming a basis for modern entropy-based thermal design.

Recent works have focused on second-grade and non-Newtonian fluids. Ramesh and Ojjela [33] reported that natural convection of viscoelastic fluids in porous systems enhances entropy due to strong coupling between flow and heat transfer. Rashidi et al. [34] demonstrated that turbulent corrugated channels increase entropy despite improved thermal performance. Shah et al. [35] investigated Hall current and electrical MHD effects in squeezing nanofluids and found that entropy grows under strong magnetic and viscous influences. Sheikhzadeh et al. [36] and Shojaeian and Kosar [37] examined turbulent nanofluid systems and identified nanoparticle type, slip effects, and dissipation as dominant entropy drivers. Similarly, Suresh et al. [38] studied hybrid nanofluids prepared by two-step methods and linked physical properties to entropy trends. Finally, Tsang and Tsang [39] presented an early channel model for fractured media, while Turkyilmazoglu [40] and Upreti et al. [41] investigated rotating disks and unsteady hybrid squeezing flows, respectively, concluding that entropy is highly dependent on rotation speed and viscous effects. Xie and Jian [42]analyzed electroosmotic nanofluid flow in layered microchannels and highlighted the importance of channel size and electrokinetic effects in entropy generation. Collectively, these works underline entropy generation as a central parameter for assessing and improving energy efficiency across diverse thermal systems. Motivated by these works, the present study focuses on analyzing entropy generation in magneto-rotational hybrid nanofluid flow under convective conditions through a porous medium-a scenario that remains largely unexplored in the current literature.The selection of silver (Ag) and aluminium oxide (Al_2O_3) nanoparticles is motivated by their complementary thermal characteristics-Ag provides extremely high thermal conductivity while (Al_2O_3) enhances suspension stability. Their combined use yields a hybrid nanofluid with superior heat transfer capability compared to traditional mono-nanofluids.

The following key questions guide the research:

- How does the suspension of silver and aluminum oxide nanoparticles in water influence the momentum and thermal transport properties of the hybrid nanofluid?
- What is the impact of porous medium resistance and Darcy dissipation on the momentum boundary layer of the hybrid nanofluid?
- How does Darcy dissipation contribute to the overall energy balance, entropy generation and Bejan number in the system?
- In what way do magnetic and slip boundary conditions modify the velocity and temperature fields of the silver-aluminium oxide/water hybrid nanofluid?
- How are engineering quantities such as skin friction coefficient, Nusselt number, and shearwood number influenced by the inclusion of porous resistance, Darcy dissipation, and hybrid nanoparticles? Novelty: The ongoing research found it interesting because of the novel approaches described below
- The study employs a water-based hybrid nanofluid with silver and aluminum oxide nanoparticles, a combination rarely explored together for porous media applications, ensuring improved heat transfer characteristics.
- The momentum equation includes porous drag effects, providing a realistic representation of flow through porous channels, which is not commonly addressed in earlier hybrid nanofluid studies.
- The energy equation accounts for Darcy dissipation, capturing the impact of internal friction within the porous structure on temperature fields and entropy generation.

- Unlike conventional no-slip models, velocity and thermal slip conditions are incorporated at the boundaries, making the analysis more relevant for microscale and nanofluidic transport systems.
- The research emphasises entropy generation, Bejan number, skin friction, and Nusselt number under the combined influence of porous resistance, Darcy dissipation, and hybrid nanoparticles-offering a holistic view of both fluid mechanics and thermal irreversibility.

2. Mathematical Model of the Problem

We investigate the steady laminar flow of an incompressible, electrically conducting hybrid nanofluid composed of water as the base fluid with dispersed silver (Ag) and aluminum oxide (Al_2O_3) nanoparticles. The fluid is confined between two parallel plates embedded in a porous medium, and the entire system rotates uniformly about the vertical axis with constant angular velocity. A uniform magnetic field is applied perpendicular to the flow domain. The lower plate is assumed to stretch in its own plane, while both plates permit velocity and thermal slip, thereby capturing microscale surface effects. The physical model shown in Fig. 1 accounts for porous drag due to the medium, which slows down the motion, and Darcy dissipation, which enhances thermal irreversibility.

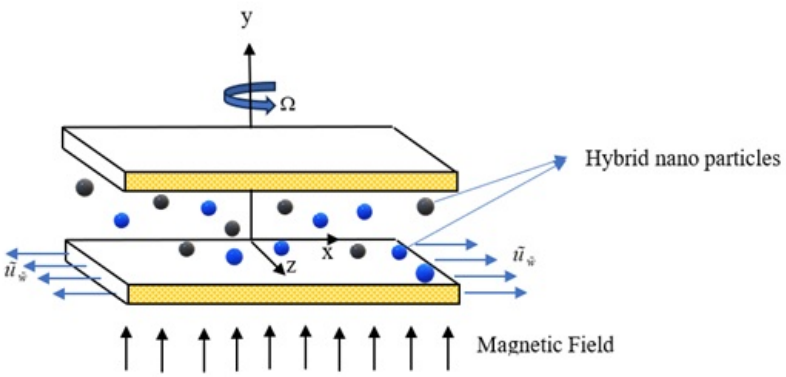

Figure 1: Effect of the velocity slip parameter h_0 and rotational parameter R_0 on velocity $f'(\eta)$

The following norms are employed in the process:

- A hybrid nanofluid made of silver (Ag) and aluminium oxide (Al_2O_3) nanoparticles dispersed in water is investigated for its high thermal conductivity and enhanced heat storage potential.
- The flow domain is assumed to be a saturated porous medium, representing practical engineering and environmental scenarios where resistance and permeability play a key role in heat and mass transport.
- The application of an external magnetic field is considered to study Lorentz force effects, which suppress fluid velocity but increase temperature and entropy generation.
- Velocity and thermal slip boundary conditions are introduced at the surface to more accurately reflect nanoscale and microscale fluid behaviour.
- Entropy generation is evaluated to quantify thermodynamic irreversibility, while the Bejan number is employed to identify whether heat transfer or viscous friction is the major contributor.

- Darcy's resistance relation is extended to account for porous media effects, emphasising its role in entropy generation and flow stability.
- Skin friction coefficient is analysed to measure surface shear stress and assess momentum transfer performance.
- The Nusselt number is computed to quantify heat transfer characteristics, reflecting the efficiency of thermal transport in the system.
- The Sherwood number is determined to evaluate mass transfer performance, highlighting the influence of porous structure and nanoparticle concentration.

The governing framework is composed of the continuity, momentum, energy, and concentration equations, each adjusted to include the effects of magnetic fields, thermal processes, and resistance from the porous medium. In the momentum balance, the porous drag is introduced through a Darcy term, which acts as a linear resistance proportional to the fluid velocity. The model further incorporates entropy generation analysis to quantify thermodynamic irreversibility arising from viscous friction, heat transfer, magnetic damping, and species diffusion. Letu, v, w be the velocity components in the x, y, z directions, respectively, and$T$ and C be the temperature and concentration. The governing mathematical model describing fluid motion inside a rotating porous channel follows the classical formulation reported by Tsang and Tsang [39]. The magnetohydrodynamic flow treatment and the application of slip-type boundary conditions in porous media are based on the methodology of Chamkha [8]. In this study, velocity slip is imposed to represent partial adherence between the fluid and channel walls, while thermal slip accounts for finite thermal resistance at the solid-fluid interface. These conditions provide a more realistic description of transport phenomena in micro- and nano-scale channels. The governing dimensional equations are: the conservation of mass Equation (2.1), the conservation of momentum Equations (2.2)–(2.4), the conservation of energy Equation (2), and the diffusion Equation (2.6).

Conservation of mass equation:

$$\frac{\partial u}{\partial x}+\frac{\partial v}{\partial y}=0 \tag{2.1}$$

Conservation of momentum equations:

$$u\frac{\partial u}{\partial x}+v\frac{\partial u}{\partial y}-2\Omega w=-\frac{1}{\rho_{hnf}}\frac{\partial p}{\partial x}+\frac{\mu_{hnf}}{\rho_{hnf}}\left(\frac{\partial^2 u}{\partial x^2}+\frac{\partial^2 u}{\partial y^2}\right)-\frac{\sigma_{hnf}B_0^2}{\rho_{hnf}}u-\frac{\mu_{hnf}}{\rho_{hnf}k_p^*}u \tag{2.2}$$

$$u\frac{\partial v}{\partial x}+v\frac{\partial v}{\partial y}=-\frac{1}{\rho_{hnf}}\frac{\partial p}{\partial y}+\frac{\mu_{hnf}}{\rho_{hnf}}\left(\frac{\partial^2 v}{\partial x^2}+\frac{\partial^2 v}{\partial y^2}\right) \tag{2.3}$$

$$u\frac{\partial w}{\partial x}+v\frac{\partial w}{\partial y}+2\Omega u=\frac{\mu_{hnf}}{\rho_{hnf}}\left(\frac{\partial^2 w}{\partial x^2}+\frac{\partial^2 w}{\partial y^2}\right)-\frac{\sigma_{hnf}B_0^2}{\rho_{hnf}}w-\frac{\mu_{hnf}}{\rho_{hnf}k_p^*}w \tag{2.4}$$

Conservation of Energy equation:

$$u\frac{\partial T}{\partial x}+v\frac{\partial T}{\partial y}=\frac{k_{hnf}}{(\rho C_p)_{hnf}}\left(\frac{\partial^2 T}{\partial x^2}+\frac{\partial^2 T}{\partial y^2}\right)+\frac{16\sigma^* T_0^3}{3k^*(\rho C_p)_{hnf}}\left(\frac{\partial^2 T}{\partial x^2}+\frac{\partial^2 T}{\partial y^2}\right)+\frac{Q_0}{(\rho C_p)_{hnf}}(T-T_0) \tag{2.5}$$

$$+\frac{\sigma_{hnf}B_0^2}{\rho_{hnf}}(u^2+w^2)+\frac{\mu_{hnf}}{(\rho C_p)_{hnf}k_p^*}(u^2+w^2)$$

Diffusion equation:

$$u\frac{\partial C}{\partial x}+v\frac{\partial C}{\partial y}=D_B\left(\frac{\partial^2 C}{\partial x^2}+\frac{\partial^2 C}{\partial y^2}\right)-k_r^2(C-C_0)\left(\frac{T}{T_0}\right)^n e^{-\frac{E_1}{kT}} \tag{2.6}$$

With boundary conditions

$$\left.\begin{aligned} u = ax + \lambda_1 \frac{\partial u}{\partial y}, \quad v = 0, \quad w = \lambda_1 \frac{\partial w}{\partial y}, \quad T = T_H + \lambda_2 \frac{\partial T}{\partial y}, \quad C = C_H \qquad \text{at } y = 0, \\ u = -\lambda_1 \frac{\partial u}{\partial y}, \quad v = 0, \quad w = -\lambda_1 \frac{\partial w}{\partial y}, \quad T = T_0 - \lambda_2 \frac{\partial T}{\partial y}, \quad C = C_0 \qquad \text{at } y = H \end{aligned}\right\} \tag{2.7}$$

The mathematical formulation is based on the Tiwari-Das homogeneous nanofluid framework, while the velocity and thermal slip boundary conditions follow the classical Navier slip approach commonly used in microscale transport modelling. This model shows how rotation, magnetic forces, temperature and concentration differences, and porous resistance affect the hybrid nanofluid. The next step is to make the equations dimensionless and solve them using MATLAB's bvp4c solver. Radiative heat transfer, as modelled by the Rosseland diffusion approximation, is described by the following relation.

$$q_r = -\frac{4\sigma}{3k^*}\left(\frac{\partial T^4}{\partial y}\right)$$

Ignoring higher-order terms, the Taylor series expansion of T^4 in terms of T_0 is

$$T^4 = -3T_0^4 + 4T_0^3 T$$

3. Thermophysical Attributes of Hybrid Nanofluid

In this study, the hybrid nanofluid is modelled using the Tiwari-Das single-phase mixture model, in which the effective density, viscosity, thermal conductivity, and heat capacity are calculated using the nanoparticle volume fractions. Since we are working with Silver (Ag) and Aluminium oxide (Al_2O_3) nanoparticles in the base fluid, hybrid nanofluid density and heat capacitance are described as

$$\frac{\rho_{hnf}}{\rho_f} = \phi_{p2}\frac{\rho_{p2}}{\rho_f} + \left[(1-\phi_{p2}) + \phi_{p1}\frac{\rho_{p1}}{\rho_f}\right](1-\phi_{p2}) \tag{3.1}$$

$$\frac{(\rho C_p)_{hnf}}{(\rho C_p)_f} = (1-\phi_{p2})\left[(1-\phi_{p1}) + \phi_{p1}\frac{(\rho C_p)_{p1}}{(\rho C_p)_f}\right] + \phi_{p2}\frac{(\rho C_p)_{p2}}{(\rho C_p)_f} \tag{3.2}$$

The hybrid nanofluid's effective thermal conductivity (k_{hnf}) is

$$\frac{k_{hnf}}{k_f} = \frac{\frac{k_{p1}\phi_{p1}+k_{p2}\phi_{p2}}{\phi_{p1}+\phi_{p2}} + 2k_f + 2(k_{p1}\phi_{p1}+k_{p2}\phi_{p2}) - 2(\phi_{p1}+\phi_{p2})k_f}{\frac{k_{p1}\phi_{p1}+k_{p2}\phi_{p2}}{\phi_{p1}+\phi_{p2}} + 2k_f - 2(k_{p1}\phi_{p1}+k_{p2}\phi_{p2}) + (\phi_{p1}+\phi_{p2})k_f} \tag{3.3}$$

The dynamic viscosity of the hybrid nanofluid (μ_{hnf}) is

$$\frac{\mu_{hnf}}{\mu_f} = \frac{1}{(1-\phi_{p1}-\phi_{p2})^{2.5}} \tag{3.4}$$

The electric conductivity of the nanofluid is

$$\frac{\sigma_{hnf}}{\sigma_f} = 1 + \frac{3\left(\sigma_{p1}\phi_{p1} + \sigma_{p2}\phi_{p2}\right)/\sigma_f - 3\left(\phi_{p1}+\phi_{p2}\right)}{2 + \left\{\frac{\sigma_{p1}\phi_{p1}+\sigma_{p2}\phi_{p2}}{(\phi_{p1}+\phi_{p2})\sigma_f}\right\} - \left\{\frac{\sigma_{p1}\phi_{p1}+\sigma_{p2}\phi_{p2}}{\sigma_f} - (\phi_{p1}+\phi_{p2})\right\}} \tag{3.5}$$

The primary and secondary nanoparticles, Silver (S_1)and Aluminium oxide(S_2), are represented by the variables S_1 and S_2. The base fluid is indicated by the subscript f, a nanofluid containing a single type of nanoparticle is denoted by$f$, and a hybrid nanofluid with two nanoparticles and a base fluid is represented by hnf. In this work, the shape of the nanoparticles is described by the form factor S, defined as$S = 3/\psi$, where represents the sphericity of the nanoparticles. The thermal conductivity of the hybrid nanofluid is modelled using the Hamilton-Crosser model ($khnf$), which is widely applied to predict the effective

Table 1: **Thermophysical properties of nanomaterials and base fluid.**

Property	Water	Silver	Aluminium oxide
ρ (kg/m^3)	9.877×10^2	$10,500$	3970
Cp (J/kg.K)	4.066×10^3	235	765
k (W / m.K)	6.44×10^{-1}	429	40
σ (m^{-1})	5.0×10^{-2}	6.30×10^7	16.7

properties of composite materials and follows a similar structure. A complete list of the thermophysical properties of the base fluid and nanoparticles [38] and [14] is provided in Table 1

The following similarity transformations are considered

$$u = axf'(\eta), v = -ahf(\eta), w = axg(\eta), \theta = \frac{T - T_0}{T_H - T_0}, \phi = \frac{C - C_0}{C_H - C_0}, \eta = \frac{y}{h} \tag{3.6}$$

By applying the transformation given in the equation (2.7), equation (2.1) is automatically satisfied, while equations (2.2)–(2.6) are simplified and reduced into the following form.

$$f''' + B_1(1-\phi_{p1}-\phi_{p2})^{2.5}\mathrm{Re}\left(f'''f'' - f'^2\right) + 2B_1(1-\phi_{p1}-\phi_{p2})^{2.5}R_0 g' - \mathrm{MnRe}B_2(1-\phi_{p1}-\phi_{p2})^{2.5}f'' = 0 \tag{3.7}$$

$$g''(\eta) - \mathrm{MnRe}B_2(1-\phi_{p1}-\phi_{p2})^{2.5}g - Da.g + B_1(1-\phi_{p1}-\phi_{p2})^{2.5}\mathrm{Re}\left(fg' - f'g\right) - 2B_1(1-\phi_{p1}-\phi_{p2})^{2.5}R_0 f' = 0 \tag{3.8}$$

$$\theta''(\eta) + \left(\frac{3}{3B_3 + 4N}\right)(\mathrm{PrRe})\left[Q^*\theta(\eta) + \mathrm{EcMn}B_2((f')^2 + g^2) + \frac{\mathrm{DaEc}}{\mathrm{Re}}(1-\phi_{p1}-\phi_{p2})^{2.5}((f')^2 + g^2) + B_4 f(\eta)\theta'(\eta)\right] = 0 \tag{3.9}$$

$$\phi''(\eta) + \mathrm{ReLe}f(\eta)\phi'(\eta) - \alpha_0\mathrm{ReLe}\phi(\eta)(1+\delta\theta)^n e^{\frac{-E_a}{1+\delta\theta}} = 0 \tag{3.10}$$

$$\begin{gathered} f(0) = 0, f'(0) = 1 + h_0 f''(0), g(0) = h_0 g'(0), \theta(0) = 1 + h_1\theta'(0), \phi(0) = 1 \text{ at } \eta = 0, \\ f(1) = 0, f'(1) = -h_0 f''(1), g(1) = -h_1 g'(1), \theta(1) = -h_1\theta'(1), \phi(1) = 0 \text{ at } \eta = 1 \end{gathered} \tag{3.11}$$

$$(\text{Prandtl number})\,\mathrm{Pr} = \frac{Cp\mu_f}{k_f}, \quad (\text{Eckert number})\,\mathrm{Ec} = \frac{a^2x^2}{(T_H - T_0)Cp_f}, \quad (\text{Reynolds number})\,\mathrm{Re} = \frac{ah^2\rho_f}{\mu_f},$$

$$(\text{Activation Energy})\,\mathrm{Ea} = \frac{E_i}{kT_0}, \quad (\text{Lewis number})\,\mathrm{Le} = \frac{\mu_f}{\rho_f D_B},$$

$$(\text{magnetic parameter})\,\mathrm{Mn} = \frac{\sigma_f B_0^2}{a\rho_f}, \quad (\text{rotation parameter})\,\mathrm{Ro} = \frac{\Omega h^2\rho_f}{\mu_f}, \quad (\text{radiation parameter})\,N = \frac{4\sigma^* T_H^3}{k^* k_f},$$

$$(\text{heat generation/absorption parameter})\,Q^* = \frac{Q_0}{(\rho Cp)_f a}, \quad (\text{velocity slip parameter})\,h_0 = \frac{\lambda_1}{h},$$

$$(\text{thermal slip parameter})\,h_1 = \frac{\lambda_2}{h}, \quad (\text{temperature ratio})\,\delta = \frac{T_H - T_0}{T_0},$$

$$(\text{chemical reaction parameter})\,\alpha_0 = \frac{k_r^2}{a},$$

4. Mathematical Formulation of Entropy Generation

This part calculates the entropy generation rate using the velocity and temperature results obtained earlier. The calculation includes the effects of heat transfer, fluid friction, Joule heating, viscous dissipation, and resistance from the porous medium (Darcy effect).

$$
\begin{aligned}
S''_{gen} = & \underbrace{\frac{k_f}{T_0^2}\left(\frac{k_{hnf}}{k_f}+\frac{16\epsilon^* T_0^3}{3k_f k^*}\right)\left[\left(\frac{\partial T}{\partial \alpha}\right)^2+\left(\frac{\partial T}{\partial \gamma}\right)^2\right]}_{\text{heat transfer irreversibility}} \\
& + \underbrace{\frac{\sigma_{hnf}B_0^2}{T_0}(u^2+w^2)}_{\text{Joule heating irreversibility}} \\
& + \underbrace{\frac{RD}{T_0}\left(\frac{\partial C}{\partial \alpha}\frac{\partial T}{\partial \alpha}+\frac{\partial C}{\partial \gamma}\frac{\partial T}{\partial \gamma}\right)\left[\left(\frac{\partial C}{\partial \alpha}\right)^2+\left(\frac{\partial C}{\partial \gamma}\right)^2\right]+\frac{RD}{C_0}}_{\text{heat transfer irreversibility}} \\
& + \underbrace{\frac{\mu_{hnf}}{T_0}\Phi}_{\text{viscous dissipation irreversibility}} + \underbrace{\frac{\mu_{hnf}}{T_0}\frac{(u^2+w^2)}{k_p^*}}_{\text{porous media irreversibility}}
\end{aligned}
\tag{4.1}
$$

where

$$
\Phi = 4\left[\left(\frac{\partial u}{\partial x}\right)^2+\left(\frac{\partial v}{\partial x}+\frac{\partial u}{\partial y}\right)^2+\left(\frac{\partial w}{\partial x}\right)^2+\left(\frac{\partial w}{\partial y}\right)^2\right],
$$

and R is the universal gas constant.
The non-dimensional form of Equation (2) is:

$$
\begin{aligned}
S''_{gen} = E_{Go}\Bigg\{ & \left(B_3+\frac{4N}{3}\right)\left(\alpha_1\theta'^2\right)+Br\cdot Mn\cdot Re\cdot B_2(f'^2+g'^2)+L\phi'\theta' \\
& +\frac{L\alpha_2}{\alpha_1}\phi'^2+\left(\frac{\mu_{hnf}}{\mu_f}\right)Br_1\left(4\left(f''(\eta)\right)^2+(g')^2\right) \\
& +\left(\frac{\mu_{hnf}}{\mu_f}\right)Br_1\left[(f''(\eta))^2+(g')^2\right]+\left(\frac{\mu_{hnf}}{\mu_f}\right)Br_1 Da(f'^2+g'^2)\Bigg\}
\end{aligned}
\tag{4.2}
$$

where:

$$
E_{Go}=\frac{k_f(T_H-T_0)}{T_0^2h^2},\quad \alpha_1=\frac{T_H-T_0}{T_0},\quad \alpha_2=\frac{C_H-C_0}{C_0},\quad L=\frac{RD(C_H-C_0)}{k_f},
$$
$$
Br_i=\frac{\mu_f a^2h^2}{k_f(T_H-T_0)},\quad Br=\frac{\mu_f a^2\lambda^2}{k_f(T_H-T_0)},\quad Da=\frac{h^2}{k_p^*}.
$$

5. Bejan Number

We have,

$$
\text{Bejan number}=\frac{\text{Heat and mass irreversibility}}{\text{the irreversibility due to heat transfer and friction}}
$$

Hence,

$$
\begin{aligned}
\text{Bejan number} = & \frac{\left(B_3+\frac{4N}{3}\right)\alpha_1\theta'^2+L\phi'\theta+\frac{L\alpha_2}{\alpha_1}\phi'^2}{\left(B_3+\frac{4N}{3}\right)\alpha_1\theta'^2+Br\,Mn\,Re\,B_2(f'^2+g^2)+L\phi'\theta} \\
& +\frac{L\alpha_2}{\alpha_1}\phi'^2+\left(\frac{\mu_{hnf}}{\mu_f}\right)Br_1\left[4(f'(\eta))^2+g^2\right]+\left(\frac{\mu_{hnf}}{\mu_f}\right)BrDa\frac{(f'^2+g^2)}{k_p^*}
\end{aligned}
$$

6. Flow Chart for Numerical Computation

MATLAB's bvp4c solver is used to numerically solve the system of highly nonlinear ordinary differential equations, which are represented by equations (2) through (6). According to equation (7), these equations are solved together with the matching boundary conditions. Equations (14) through (17) represent the system of ODEs, and equations (18) represent the boundary conditions. These are then reformed into a set of first-order linear equations. Initial approximations that meet the asymptotic boundary requirements are carefully chosen to guarantee the accuracy of the solution. Next, several variables are introduced, including: The ordinary differential equations given by Eqs. (14) through (17), we solve the problem in MATLAB in the following way.

$$
\begin{aligned}
f' &= y(2);\\
f'' &= y(3);\\
f''' &= y(4);\\
f'''' &= B_1(1-\phi_{p1}-\phi_{p2})^{2.5}\, Re\,(y(2)y(3)-y(1)y(4)) - 2B_1R_0\big((1-\phi_{p1}-\phi_{p2})^{2.5}\big)y(6)\\
&\quad + Mn\, Re\, B_2(1-\phi_{p1}-\phi_{p2})^{2.5}y(3);\\
g' &= y(6);\\
g'' &= B_1(1-\phi_{p1}-\phi_{p2})^{2.5}\, Re\,(y(2)y(5)-y(1)y(6)) - 2B_2R_0\big((1-\phi_{p1}-\phi_{p2})^{2.5}\big)y(2)\\
&\quad + Mn\, Re\, B_2(1-\phi_{p1}-\phi_{p2})^{2.5}y(5) + Da_\alpha y(5);\\
\theta' &= y(8);\\
\theta'' &= -(Pr\, Re)\left(\frac{3}{(3B_3+4N)}\right)\Bigg[B_4y(1)y(8) + Mn\, Ec\, B_2\left\{(y(2))^2+(y(5))^2\right\}\\
&+ \quad \frac{Da\, Ec}{Re}(1-\phi_{p1}-\phi_{p2})^{2.5}\left((y(2))^2+(y(5))^2\right) + Q\, y(7)\Bigg];\\
\phi' &= y(10);\\
\phi'' &= -Re\, Le\, y(1)y(10) + \alpha_0 Re\, Le(1+y(7))\,\delta\,\exp\left(\frac{-E_a}{1+y(7)/\gamma}\right)y(9).
\end{aligned}
$$

7. Quantities of Interest

In fluid dynamics, the force of friction that a flowing fluid applies to a surface is referred to as skin friction. The Nusselt number, a non-dimensional statistic, is used to measure how well convective heat transfer works in fluid surface flow. The coefficient of skin friction (C_{f}) ,the Nusselt number(Nu) and the Sherwood number(Sh) at the lower plate are determined in this section:

7.1. Surface drag force

Skin friction coefficient is defined as

$$C_f = \frac{\mu_{hnf}}{\rho_{hnf}v_0^2}\left(\frac{\partial u}{\partial y}\right)_{y=0} = \frac{\mu_{hnf}}{\mu_f}\frac{\rho_f}{\rho_{hnf}}\frac{\mu_f}{\rho_f v_0^2}\cdot\frac{\alpha x f''(0)}{h} \tag{22}$$

The local skin-friction coefficient is expressed as

$$C_f\sqrt{Re_x} = \left(\frac{\mu_{hnf}}{\mu_f}\right)\left(\frac{\rho_f}{\rho_{hnf}}\right)f''(0) \tag{23}$$

7.2. Nusselt number

The Nusselt number is given by

$$Nu^* = \frac{hk_f}{(T_H - T_0)} \left(\frac{k_{hnf}}{k_f} + \frac{16\epsilon^* T_0^3}{3k_f k^*} \right) \left(\frac{\partial T}{\partial y} \right)_{y=0} \tag{24}$$

The dimensionless Nusselt number is expressed as

$$Nu_x \sqrt{Re_x} = \left(\frac{k_{hnf}}{k_f} + \frac{4}{3} N \right) \theta'(0) \tag{25}$$

7.3. Sherwood number

It is given by

$$Sh^* = \frac{-h}{(C_H - C_0)} \left. \frac{\partial C}{\partial y} \right|_{\eta=0} \tag{26}$$

$$Sh_x \sqrt{Re_x} = \phi'(0) \tag{27}$$

8. Result and Discussion

This section presents the outcomes of the numerical investigation concerning the influence of various dimensionless parameters on the velocity components, temperature, and concentration fields in a hybrid nanofluid system confined within a porous rotating channel under magnetic effects.These physical parameters are employed in the range of $5 < Pr < 7,\ 1 < Le < 5,\ 0 \leq Mn < 6,\ 0.01 < Da \leq 1,\ 0.01 < Ec \leq 1,\ 0 \leq N \leq 2,\ -1 \leq Q \leq 1,\ 0 \leq \lambda_1 \leq 1,\ 0 \leq \lambda_2 \leq 1,\ 0 \leq R_0 \leq 3,\ 0 \leq \alpha_0 \leq 2,\ 1 \leq Ea \leq 10,\ 0.1 \leq \delta \leq 1,\ 1 \leq Sc \leq 5,\ 1 \leq Re \leq 100$.

From Figs. 2–4 , it is clear that both the slip parameter h_0 and the rotational parameter R_0 reduce the velocity and its gradients. In Fig. 2, the velocity gradient $f'(\eta)$ decreases when h_0 increases, meaning the shear stress at the wall becomes weaker because the fluid slides more easily instead of sticking to the surface. A similar decreasing trend is seen with higher R_0, since rotation introduces a Coriolis-type resistance that slows down the fluid and reduces momentum transfer.

In Fig. 3, the main velocity $f(\eta)$ also goes down with increasing slip and rotation, showing that the flow weakens as the wall-fluid interaction reduces and rotational forces oppose motion. In Fig. 4, the secondary velocity component $g(\eta)$ becomes smaller under higher slip and rotation, confirming that both parameters act as resistive effects. Physically, this means that slip reduces the frictional control of the wall on the fluid, while rotation adds an opposing force, and together they cause thinner boundary layers, weaker shear, and lower fluid velocities.

From Figs. 5–7, it is evident how the magnetic parameter Mn and the Darcy number Da influence the flow velocities. In Fig. 5, the velocity gradient $f'(\eta)$ decreases with larger Mn, which means the magnetic field slows down the fluid motion because the Lorentz force acts as a drag force opposing the flow. On the other hand, when the Darcy number increases, the velocity gradient becomes stronger since a larger Da reduces the resistance of the porous medium and allows the fluid to pass more easily.

In Fig. 6, the main velocity $f(\eta)$ shows a clear reduction with higher Mn, again confirming that the magnetic field resists the motion, while higher Da increases the velocity since permeability improves the flow through the medium. Similarly, in Fig. 7, the secondary velocity $g(\eta)$ decreases as Mn increases, indicating that the magnetic field suppresses both primary and secondary flows, whereas higher Darcy number helps maintain larger velocity values.

Physically, this means that the magnetic parameter acts like a resistive force that slows the fluid by generating opposing currents, while the Darcy number represents the porous structure, where larger Da reduces drag from the medium and allows easier motion. Together, Mn suppresses the flow while Da enhances it, leading to competing effects on the velocity profiles. Conversely, a rise in the Darcy number (Da) causes a significant increase in f', f, and g, as it represents higher permeability of the porous medium. With less resistance from the solid matrix, the fluid accelerates more freely, enhancing both streamwise and cross-flow velocities.

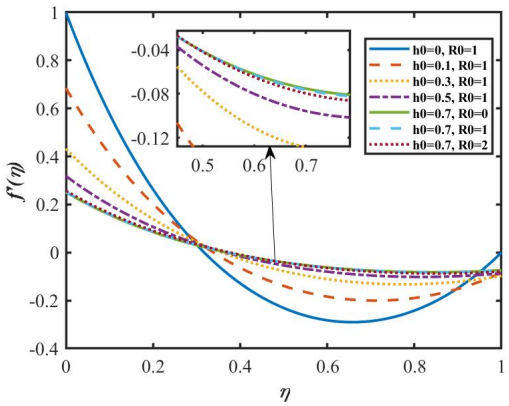

Figure 2: Effect of the velocity slip parameter h_0 and rotational parameter R_0 on velocity $f'(\eta)$

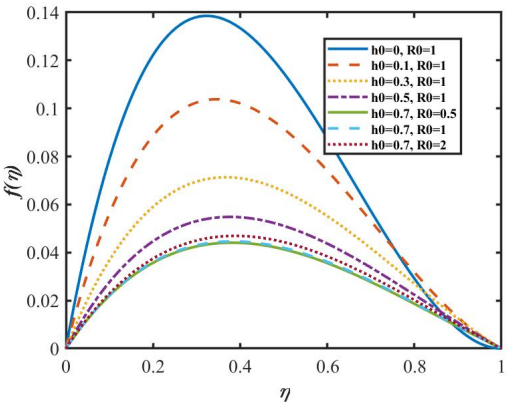

Figure 3: Effect of the velocity slip parameter h_0 and rotational parameter R_0 on velocity $f(\eta)$

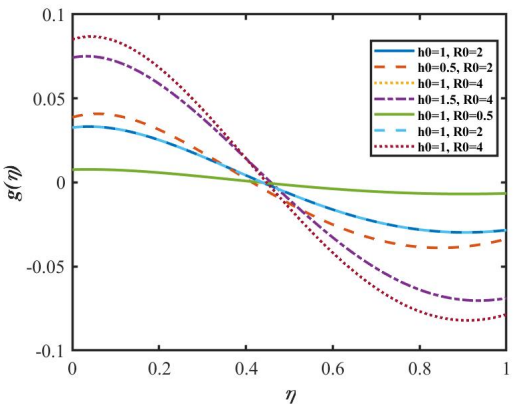

Figure 4: Effect of the velocity slip parameter h_0 and rotational parameter R_0 on velocity $g(\eta)$

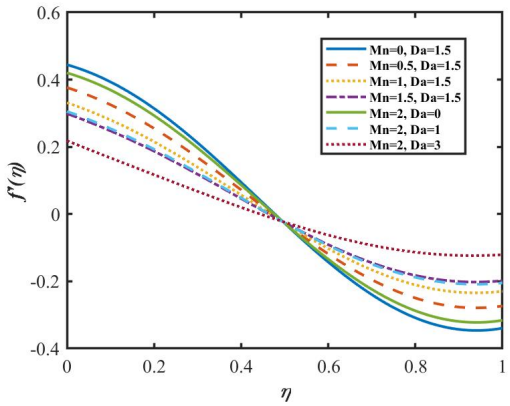

Figure 5: Effect of the magnetic parameter Mn and Darcy number Da on velocity $f'(\eta)$.

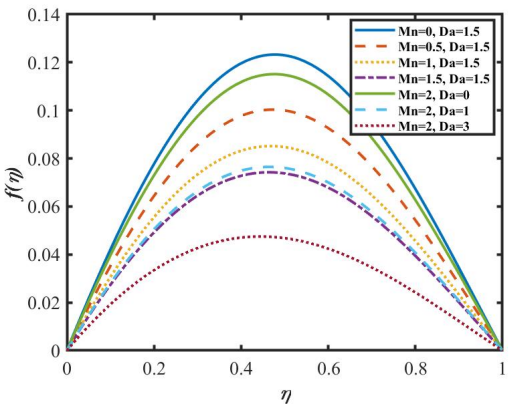

Figure 6: Effect of the magnetic parameterMn and Darcy number Da on velocity $f(\eta)$

In Fig. 8, the temperature profile decreases with an increase in the magnetic parameter Mn and the thermal slip parameter h_1. The magnetic field generates a Lorentz force that resists fluid motion and reduces convective heat transport, while thermal slip weakens the wall's ability to transfer heat to the fluid; together, both effects lower the boundary layer temperature. In Fig. 9, the temperature rises with a higher Eckert number Ec because viscous dissipation converts kinetic energy into heat, whereas it decreases with a larger Darcy number Da since a more permeable porous medium allows heat to dissipate more effectively. These results show that Mn and h_1 contribute to cooling, Ec leads to heating, and Da enhances cooling, offering useful ways to control temperature in thermal systems and porous medium applications.The presence of $Ag$and Al_2O_3 nanoparticles significantly improves the thermal conductivity of the fluid, which intensifies heat transfer, reduces the thermal boundary layer thickness, and modifies the temperature distribution inside the porous rotating channel.

In Fig. 10, the diffusion profile $\phi(\eta)$ decreases more rapidly when the Eckert number Ec takes negative values, as less energy is available for molecular motion, while a larger Darcy number Da slightly enhances diffusion because higher permeability in the porous medium allows solute to spread more easily.In Fig. 11, both the Lewis number Le and the chemical reaction parameter α_0 reduces the concentration profile, since stronger mass diffusivity relative to heat transfer Le and higher chemical reaction rate α_0 cause faster decay of species in the boundary layer. These results show that Ec and Da mainly govern how energy

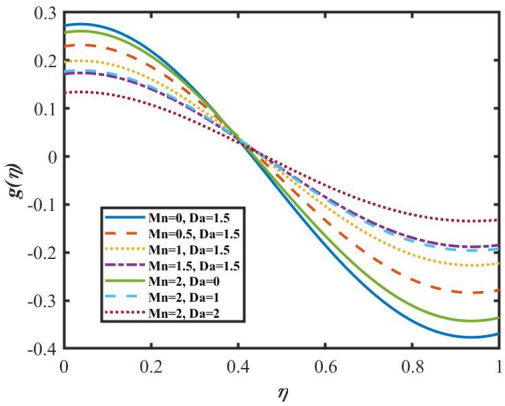

Figure 7: Effect of the magnetic parameter$Mn$and Darcy numberDa on velocity$g(\eta)$.

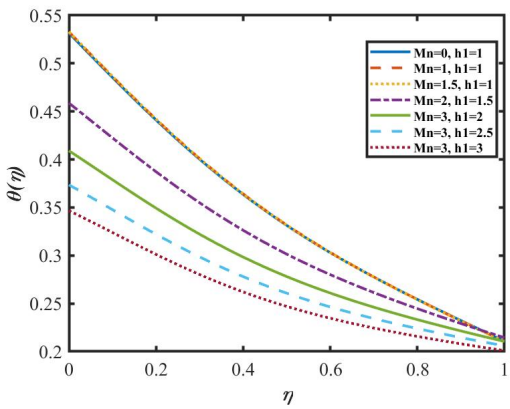

Figure 8: Effect of the magnetic parameterMn and thermal slip parameterh_0 on temperature $\theta(\eta)$.

and porous effects influence diffusion, whereas Le and α_0 control how mass transfer and reaction reduce concentration, which is important in chemical reactor design, porous medium transport, and industrial mass transfer systems. parameter $\alpha_0$reduce the concentration profile, since stronger mass diffusivity relative to heat transfer Le and higher chemical reaction rate α_0 cause faster decay of species in the boundary layer. These results show that Ec and Da mainly govern how energy and porous effects influence diffusion, whereas Le and α_0 control how mass transfer and reaction reduce concentration, which is important in chemical reactor design, porous medium transport, and industrial mass transfer systems.

8.1. Validation

The Nusselt number results were verified using the thermophysical properties documented by Ijaz Khan [21], in the absence of both Darcy and its dissipation effects.

In Table 2, the variation of the local Nusselt number with the governing parameters shows clear physical trends. An increase in the Prandtl number leads to higher values of $Nu_x\sqrt{Re_x}$ (less negative), since a larger Pr reduces thermal diffusivity, thins the thermal boundary layer, and enhances the wall temperature gradient, thereby strengthening heat transfer. The magnetic parameter also raises $Nu_x\sqrt{Re_x}$ in the present regime, as the Lorentz force slows the flow but the accompanying Joule heating elevates

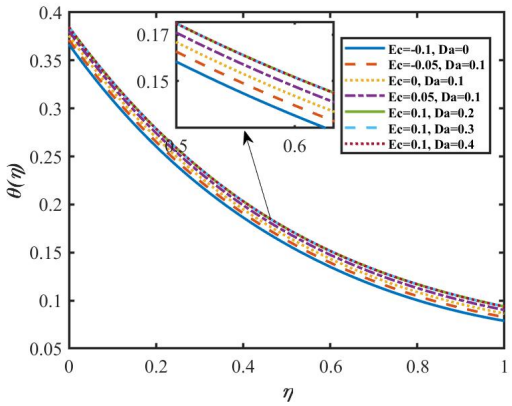

Figure 9: Effect of the Eckert number Ec and Darcy number Da on temperature$\theta(\eta)$.

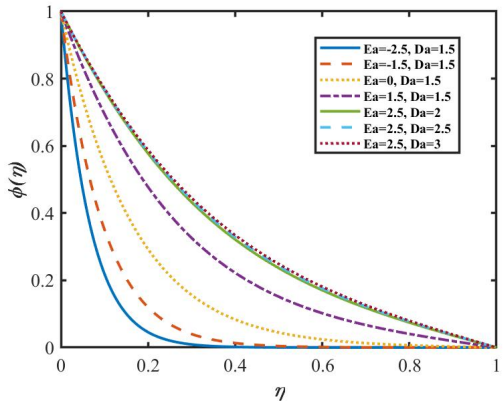

Figure 10: Effect of the Eckert number Ec and Darcy number Daon diffusion$\Phi(\eta)$.

near-wall temperatures, producing a stronger thermal gradient that outweighs the retarding effect. By contrast, an increase in the Eckert number causes a reduction in heat flux $Nu_x\sqrt{Re_x}$, because viscous dissipation converts kinetic energy into internal energy, raising the fluid temperature inside the boundary layer and thereby reducing the heat flux at the wall. The effect of the parameter N is non-monotonic at lower to moderate values, as it increases the Nusselt number by promoting enhanced thermal transport. However, at higher values, it decreases the Nusselt number due to thermal accumulation or flow resistance that thickens the thermal boundary layer. These observations confirm that heat transfer in the system is strongly governed by the interplay between fluid properties, magnetic damping, viscous heating, and thermal transport mechanisms.

9. Entropy Generation Number

The variation of the entropy generation number ($\mathrm{N_G}$) as a function of different parameters, including Da (Darcy number), Mn (magnetic number), Ec (Eckert number), and N (radiation parameter). The $Ag - Al_2O_3$ nanoparticles affect the thermal behaviour of the fluid. Silver transfers heat very quickly because it has very high thermal conductivity, while aluminium oxide helps keep the fluid stable and prevents the particles from sticking together. When these two nanoparticles are mixed, the resulting

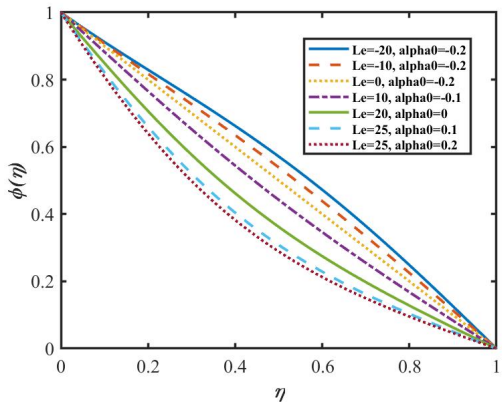

Figure 11: Effect of the Lewis numberLe and Chemical reaction parameter α_0 on diffusion $\Phi(\eta)$.

Table 2: Comparison for $Nu_x\sqrt{Re_x}$

Pr	**Mn**	**Ec**	**N**	$Nu_x\sqrt{Re_x}$	
				Ijaz Khan et al. [21]	**Present study**
6	0.6	0.2	1.3	-0.90757	-0.90756
6.2				-0.84391	-0.84391
6.4				-0.77797	-0.77798
6.2	1			-0.84087	-0.84088
	2			-0.83493	-0.83493
	5			-0.81809	-0.81810
	0.5	0.5		-0.8330	-0.8330
		1		-0.83162	-0.83162
		1.5		-0.82393	-0.82393
	0.2	1.7		-1.13684	-1.13684
		2		-1.73430	-1.73429
		2.5		-2.31665	-2.31664

hybrid nanofluid carries heat more effectively. This improved heat transfer directly affects the temperature of the fluid and the amount of entropy generated. Therefore, the thermal behaviour of the nanoparticles is now explained in the manuscript to support the entropy analysis.In Fig. 12, the entropy generation number N_{G} increases with both the Darcy number Da and the magnetic parameterMn . This means that stronger magnetic effects and more permeable porous media contribute to higher irreversibility in the system. In Fig. 13, entropy generation rises significantly when the Eckert number Ec increases, showing that viscous dissipation strongly enhances thermal irreversibility, whileDa also contributes to this rise. In Fig. 14, entropy generation increases with higher radiation parameter , as radiative heat transfer adds more thermal energy and raises entropy, while Da again supports this effect. Overall, these figures reveal that magnetic field, viscous dissipation, radiation, and porous permeability all enhance entropy generation, indicating higher irreversibility in the thermal system. This is important for thermal design because minimizing these effects can help improve energy efficiency and reduce losses in porous media heat transfer applications.

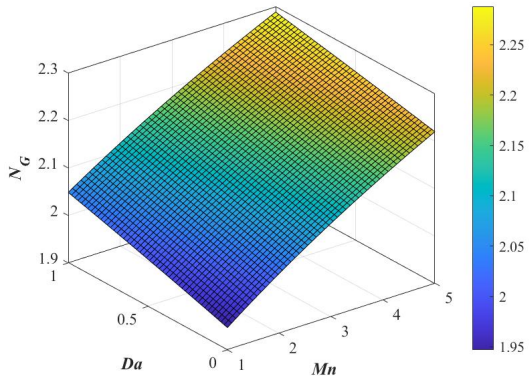

Figure 12: Variation of Entropy generation (N_G)) with Darcy number (Da) and Magnetic parameter (Mn) in Porous Media.

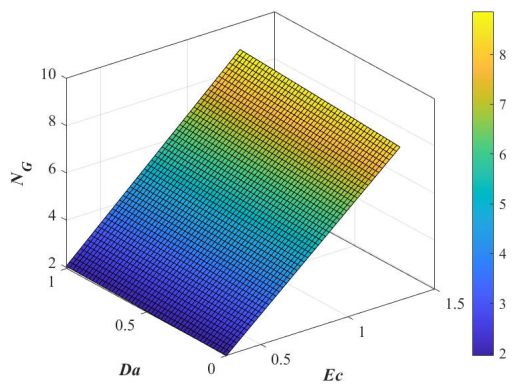

Figure 13: Variation of Entropy generation (N_G)) with Darcy number (Da) and Eckert number (Ec) in Porous Media.

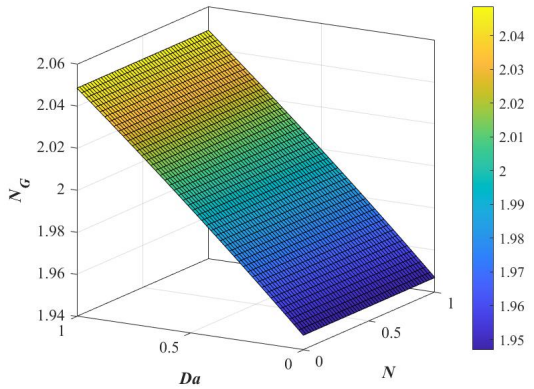

Figure 14: Variation of Entropy generation (N_G) with Darcy number (Da) and radiation parmeter (N) in Porous Media.

In Fig. 15, the Bejan number Be decreases with increasing magnetic parameterMn and increases slightly with the Darcy numberDa . This indicates that stronger magnetic fields enhance fluid friction effects, increasing entropy generation due to viscous dissipation and reducing the share of heat transfer irreversibility in the system. In contrast, higher Da (more permeable media) reduces flow resistance, slightly favouring thermal transport and thus increasing Be . In Fig. 16, Be increases with both the radiation parameter N and Da . This suggests that radiation enhances heat transfer, raising thermal entropy generation and increasing , while higher permeability again supports this trend. Overall, these figures show that magnetic fields reduce Be by increasing viscous effects, while radiation and porous permeability raise Be by promoting thermal irreversibility. These insights are crucial for optimizing thermal systems in porous media, helping engineers balance heat transfer efficiency and entropy generation.In Fig. 17, the skin friction coefficient C_{f} decreases as the magnetic parameter increases, which happens because the applied magnetic field generates a Lorentz force that resists fluid motion and lowers shear stress at the wall. On the other hand, C_{f} increases with the Darcy numberDa since a higher Darcy number reduces the drag effect of the porous medium, allowing smoother flow near the boundary and hence higher wall shear.

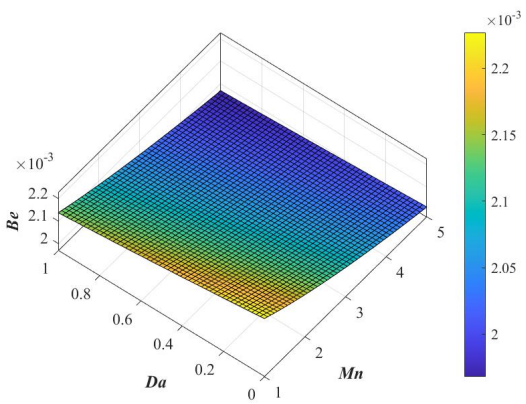

Figure 15: Variation of Bejan number (Be)) with Darcy number (Da) and magnetic parameter (Mn) in Porous Media.

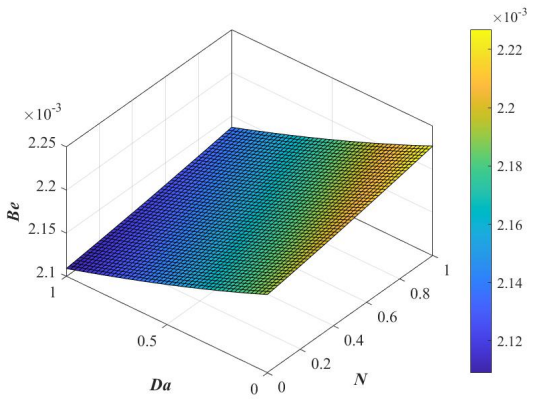

Figure 16: Variation of Bejan number (Be)) with Darcy number (Da) and radiation parmeter (N) in Porous Media.

In Fig. 18, the Nusselt number Nu shows an opposite trend: it decreases with increasing Mn , meaning the magnetic field suppresses fluid motion and reduces heat transfer. However, Nu increases with Da , as greater permeability improves fluid circulation and enhances convective heat transfer at the wall. In Fig. 19, the Sherwood number varies with both the Lewis numberLe and activation energy Eaparameter. It increases with larger Le , as stronger mass diffusivity enhances concentration gradients, but decreases with higher Ea , since activation energy slows down the diffusion process and weakens species transport.

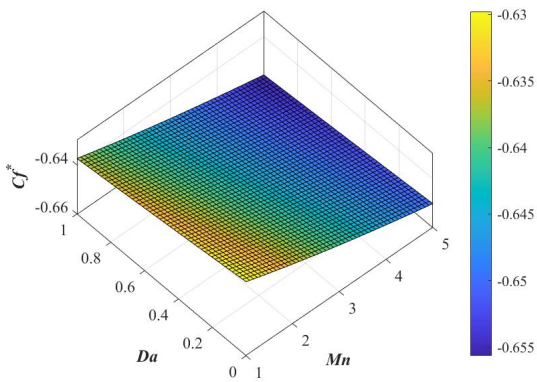

Figure 17: Variation of skin friction (C_f) with Darcy number (Da) and magnetic parameter (Mn) in Porous Media.

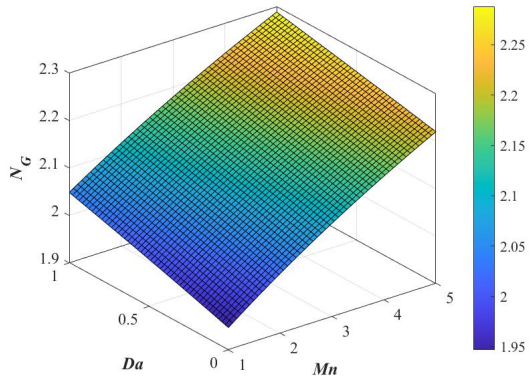

Figure 18: Variation of Nusselt number (N_u) Darcy number (Da) and magnetic parameter (Mn) in Porous Media.

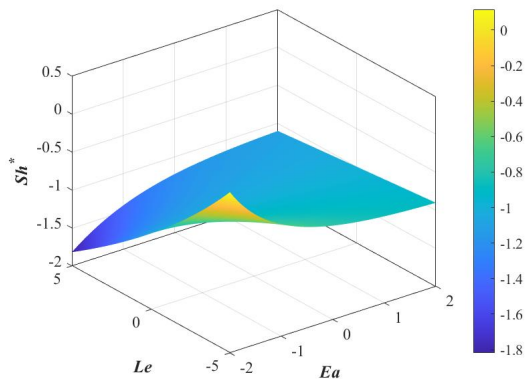

Figure 19: Variation of Sheerwood number (S_h) Darcy number (Da) and magnetic parameter (Mn) in Porous Media.

10. Results for Skin Friction

Table 3: Results for Skin Friction

Mn	**Da**	C_f^* (at $\lambda_1 = 0$ & $\lambda_2 = 0$)	C_f^* (at $\lambda_1 = 0$ & $\lambda_2 = 1$)	C_f^* (at $\lambda_1 = 1$ & $\lambda_2 = 1$)
1	0.2	-3.4603	-3.4603	-0.63138
2	0.2	-3.5408	-3.5408	-0.63711
3	0.2	-3.6197	-3.6197	-0.64232
1	0.4	-3.4815	-3.4815	-0.63294
2	0.4	-3.5616	-3.5616	-0.63852
3	0.4	-3.6402	-3.6402	-0.6436
1	0.6	-3.5027	-3.5027	-0.63445
2	0.6	-3.5823	-3.5823	-0.6399
3	0.6	-3.6605	-3.6605	-0.64486

Table 4: Results for Nusselt number

Mn	**Da**	Nu^* (at $\lambda_1 = 0$ & $\lambda_2 = 0$)	Nu^* (at $\lambda_1 = 1$ & $\lambda_2 = 0$)	Nu^* (at $\lambda_1 = 1$ & $\lambda_2 = 1$)
1	0.2	-4.4938	-4.4582	-1.5686
2	0.2	-4.3376	-4.4462	-1.5644
3	0.2	-4.1859	-4.4359	-1.5609
1	0.4	-4.4665	-4.4557	-1.5679
2	0.4	-4.3113	-4.4441	-1.5638
3	0.4	-4.1607	-4.4342	-1.5604
1	0.6	-4.4395	-4.4534	-1.5671
2	0.6	-4.2853	-4.4422	-1.5632
3	0.6	-4.1355	-4.4325	-1.5599

Table 3 illustrates the variation of the skin friction coefficient C_f^* for different values of the magnetic parameter (M_h), Darcy number (Da), and slip parameters (λ_1 and λ_2). Here, M_h quantifies the influence of the applied magnetic field, while Da characterizes the permeability of the porous medium. The slip parameters λ_1 (velocity slip) and λ_2 (thermal slip) relax the no-slip condition, allowing finite discontinuities in velocity and temperature at the wall. Negative values of C_f^* indicate reversed shear direction. Results show that for a fixed Da, increasing M_h slightly decreases $|C_f^*|$ due to the Lorentz force resisting the flow. Furthermore, the introduction of slip conditions markedly reduces surface shear stress by weakening momentum exchange at the wall.

Table 4 represents the corresponding Nusselt number (Nu^*), which measures the non-dimensional heat transfer rate, with negative values indicating heat flow opposite to the conventional gradient. Similar to C_f^*, the results indicate that higher M_h leads to a small decrease in $|Nu^*|$, reflecting the magnetic field's suppression of convective heat transport. The presence of slip parameters further reduces $|Nu^*|$, as velocity and thermal slip lessen thermal interaction between the fluid and the wall, thereby lowering the rate of heat transfer.An increase in the Lewis number reduces mass diffusion, creating a stronger concentration gradient and raising the Sherwood number. A higher activation energy slows the reaction rate and increases concentration. Radiation adds thermal energy, reducing the Nusselt number by weakening the thermal gradient. Larger Eckert number values enhance viscous heating, lowering wall heat flux. Heat generation increases internal energy and decreases heat transfer. Greater slip at the wall reduces shear stress and results in lower skin friction.

11. Conclusion

This research conducts a numerical investigation of entropy generation in MHD hybrid nanofluid flow through a porous medium with velocity and thermal slip conditions taken into account. The main findings are:

- Porous medium resistance and Darcy dissipation reduce the axial velocity profile, resulting in stronger drag forces and higher skin friction coefficients at the plate.
- The addition of silver and aluminium oxide nanoparticles enhances the effective thermal conductivity of the base fluid, which increases the Nusselt number and strengthens the overall heat transfer rate.
- Thermal boundary layer thickness decreases as nanoparticle loading improves heat transfer, while velocity boundary layer thickness rises due to porous drag.
- The Sherwood number increases with stronger porous resistance, indicating improved mass transfer characteristics and sharper concentration gradients near the wall.
- Darcy dissipation contributes to additional heat generation in the system, which intensifies temperature rise in the porous region.
- Entropy generation grows with higher Darcy drag and viscous effects, reflecting enhanced irreversibility in the flow field.

- The Bejan number analysis shows that at higher nanoparticle volume fractions, heat transfer irreversibility dominates over frictional irreversibility, signifying a thermodynamically favourable regime.
- Increasing the magnetic parameter (Mn) further resists the motion of fluid particles, leading to slower velocity but higher temperature and entropy generation due to the Lorentz force and Joule heating.
- A larger Darcy number (Da) reduces resistance inside the porous region, thereby enhancing velocity but lowering entropy generation.
- Eckert number (Ec) strengthens temperature distribution due to viscous dissipation, which enhances the Nusselt number and entropy generation simultaneously.
- A rise in Prandtl number reduces the thermal boundary layer, resulting in a decrease in fluid temperature but an improvement in Nusselt number.
- Lewis number significantly affects concentration distribution, with higher values lowering concentration boundary layer thickness and reducing Sherwood number.
- Slip parameters (velocity and thermal slip) control near-wall behaviour, where velocity slip decreases skin friction, while thermal slip reduces wall temperature gradients and weakens the Nusselt number.
- Overall, the $H_2O - Ag - Al_2O_3$ hybrid nanofluid in porous medium with Darcy dissipation offers superior heat and mass transfer compared to conventional fluids, but at the cost of higher entropy generation.

These results are significant in enhancing the application of hybrid nanofluids in heat exchangers, medical cooling systems, and energy storage systems, where entropy generation has to be minimized.

Acknowledgments

The authors acknowledge the support of REVA University and extend their thanks to the reviewers for their thoughtful and detailed comments, which strengthened the quality and rigor of this study.

References

1. Abbas, Z., Naveed, M., Hussain, M., Salamat, N., *Analysis of entropy generation for MHD flow of viscous fluid embedded in a vertical porous channel with thermal radiation.* Alexandria Eng. J. 59, 3395–3405 (2020). https://doi.org/10.1016/j.aej.2020.05.019
2. Abdelhameed, T. N., *Entropy generation analysis for mixed convection flow of nanofluid due to vertical plate with chemical reaction effects.* Sci. Rep. 13, 13279 (2023). https://doi.org/10.1038/s41598-023-39693-3
3. Al-Odat, M. Q., Damseh, R. A., Al-Nimr, M. A., *Effect of magnetic field on entropy generation due to laminar forced convection past a horizontal flat plate.* Entropy 6, 293–303 (2004). https://doi.org/10.3390/e6030293
4. Awad, M. M., *A review of entropy generation in microchannels.* Adv. Mech. Eng. 7, 1687814015590297 (2015). https://doi.org/10.1177/1687814015590297
5. Bahaidarah, H. M., *Entropy generation during fluid flow in sharp edge wavy channels with horizontal pitch.* Adv. Mech. Eng. 8, 1687814016660929 (2016). https://doi.org/10.1177/1687814016660929
6. Balamurugan, K., Sudhakar, M., Raju, V., *Entropy generation and dissipative effects on Couette flow in an aligned magnetic field with radiation and heat source.*Int. J. of Eng and Sci Inv, 7(4), 1–11(2018). https://europub.co.uk/articles/-A-396710
7. Chakraborty, R., Dey, R., Chakraborty, S., *Thermal characteristics of electromagnetohydrodynamic flows in narrow channels with viscous dissipation and Joule heating under constant wall heat flux.* Int. J. Heat Mass Transf. 67, 1151–1162 (2013). https://doi.org/10.1016/j.ijheatmasstransfer.2013.08.099
8. Chamkha, A. J., *Flow of two-immiscible fluids in porous and nonporous channels.* J. Fluids Eng. 122, 117–124 (2000). https://doi.org/10.1115/1.483233
9. Cox, S. M., *Two-dimensional flow of a viscous fluid in a channel with porous walls.* J. Fluid Mech. 227, 1–33 (1991). https://doi.org/10.1017/S0022112091000010
10. Das, S., Jana, R. N., Makinde, O. D., *MHD flow of Cu–Al_2O_3/water hybrid nanofluid in porous channel: analysis of entropy generation.* Defect Diffus. Forum 377, 42–61 (2017). https://doi.org/10.4028/www.scientific.net/DDF.377.42

11. Dawar, A., Shah, Z., Khan, W., Idrees, M., Islam, S., *Unsteady squeezing flow of magnetohydrodynamic carbon nanotube nanofluid in rotating channels with entropy generation and viscous dissipation*. Adv. Mech. Eng. 11, 1687814018823100 (2019). https://doi.org/10.1177/1687814018823100

12. Dogonchi, A. S., Waqas, M., Afshar, S. R., Seyyedi, S. M., Hashemi-Tilehnoee, M., Chamkha, A. J., Ganji, D. D., *Investigation of magnetohydrodynamic fluid squeezed between two parallel disks considering Joule heating, thermal radiation, and adding different nanoparticles*. Int. J. Numer. Methods Heat Fluid Flow 30, 659–680 (2020). https://doi.org/10.1108/HFF-05-2019-0390

13. Ebrahimi, A., Rikhtegar, F., Sabaghan, A., Roohi, E., *Heat transfer and entropy generation in a microchannel with longitudinal vortex generators using nanofluids*. Energy 101, 190–201 (2016). https://doi.org/10.1016/j.energy.2016.01.102

14. Eid, M. R., Nafe, M. A., *Thermal conductivity variation and heat generation effects on magneto-hybrid nanofluid flow in a porous medium with slip condition*. Waves Random Complex Media 32, 1103–1127 (2022). https://doi.org/10.1080/17455030.2020.1810365

15. Enamul, S., Ontela, S., *Magnetohydrodynamic Darcy–Forchheimer flow of non-Newtonian second-grade hybrid nanofluid bounded by double-revolving disks with variable thermal conductivity: entropy generation analysis*. Hybrid Adv. 6, 100226 (2024). https://doi.org/10.1016/j.hybadv.2024.100226

16. Enamul, S., Samal, S., Ontela, S., *Entropy analysis of Darcy–Forchheimer flow of couple-stress TiO_2–$CoFe_2O_4$/engine oil based hybrid nanofluid between two rotating disks considering Hall effect*. Partial Differ. Equ. Appl. Math. 13, 101073 (2025). https://doi.org/10.1016/j.padiff.2025.101073

17. Hayat, T., Qayyum, S., Khan, M. I., Alsaedi, A., *Entropy generation in magnetohydrodynamic radiative flow due to rotating disk in presence of viscous dissipation and Joule heating*. Phys. Fluids 30, 017101 (2018). https://doi.org/10.1063/1.5009611

18. Hayat, T., Razaq, A., Khan, S. A., Alsaedi, A., *Corrigendum to "An induced magnetic field utilization for hybrid nanoliquid flow subject to entropy generation"*. J. Magn. Magn. Mater. 610, 172541 (2024). https://doi.org/10.1016/j.jmmm.2024.172541

19. Hooman, K., *Entropy generation for microscale forced convection: effects of thermal boundary conditions, velocity slip, temperature jump, viscous dissipation, and duct geometry*. Int. Commun. Heat Mass Transf. 34, 945–957 (2007). https://doi.org/10.1016/j.icheatmasstransfer.2007.05.019

20. Ibáñez, G., López, A., Pantoja, J., Moreira, J., Reyes, J. A., *Optimum slip flow based on the minimization of entropy generation in parallel plate microchannels*. Energy 50, 143–149 (2013). https://doi.org/10.1016/j.energy.2012.11.036

21. Ijaz Khan, M., Hafeez, M. U., Hayat, T., Imran Khan, M., Alsaedi, A., *Magneto rotating flow of hybrid nanofluid with entropy generation*. Comput. Methods Programs Biomed. 183, 105093 (2020). https://doi.org/10.1016/j.cmpb.2019.105093

22. Ijaz Khan, M., Rahman, M. U., Khan, S. A., Hayat, T., Imran Khan, M., *Evaluation of entropy generation in cubic autocatalytic unsteady squeezing flow of nanofluid between two parallel plates*. Comput. Methods Programs Biomed. 185, 105149 (2020). https://doi.org/10.1016/j.cmpb.2019.105149

23. Khan, N. S., Shah, Q., Bhaumik, A., Kumam, P., Thounthong, P., Amiri, I., *Entropy generation in bioconvection nanofluid flow between two stretchable rotating disks*. Sci. Rep. 10, 4448 (2020). https://doi.org/10.1038/s41598-020-61172-2

24. Khan, Z. H., Khan, W. A., Tang, J., Sheremet, M. A., *Entropy generation analysis of triple diffusive flow past a horizontal plate in porous medium*. Chem. Eng. Sci. 228, 115980 (2020). https://doi.org/10.1016/j.ces.2020.115980

25. Kiyasatfar, M., *Convective heat transfer and entropy generation analysis of non-Newtonian power-law fluid flows in microchannels*. Int. J. Therm. Sci. 128, 15–27 (2018). https://doi.org/10.1016/j.ijthermalsci.2018.02.013

26. López, A., Ibáñez, G., Pantoja, J., Moreira, J., Lastres, O., *Entropy generation analysis of MHD nanofluid flow in a porous vertical microchannel*. Int. J. Heat Mass Transf. 107, 982–994 (2017). https://doi.org/10.1016/j.ijheatmasstransfer.2016.10.126

27. Mahian, O., Kianifar, A., Kleinstreuer, C., Al-Nimr, M. A., Pop, I., Sahin, A. Z., Wongwises, S., *A review of entropy generation in nanofluid flow*. Int. J. Heat Mass Transf. 65, 514–532 (2013). https://doi.org/10.1016/j.ijheatmasstransfer.2013.06.010

28. Makinde, O. D., *Free convection flow with thermal radiation and mass transfer past a moving vertical porous plate*. Int. Commun. Heat Mass Transf. 32, 1411–1419 (2005). https://doi.org/10.1016/j.icheatmasstransfer.2005.07.005

29. Manay, E., Akyürek, E. F., Sahin, B., *Entropy generation of nanofluid flow in a microchannel heat sink*. Results Phys. 9, 615–624 (2018). https://doi.org/10.1016/j.rinp.2018.03.013

30. Murshid, N., Mulki, H., Abu-Samha, M., Owhaib, W., Raju, S. S. K., Raju, C. S. K., Jayachandra Babu, M., Homod, R. Z., Al-Kouz, W., *Entropy generation and statistical analysis of MHD hybrid nanofluid unsteady squeezing flow between two parallel rotating plates with activation energy*. Nanomaterials 12, 2381 (2022). https://doi.org/10.3390/nano12142381

31. Murugan, R. D., Sivakumar, N., Tarakaramu, N., Ahmad, H., Askar, S., *Entropy generation on MHD motion of hybrid nanofluid with porous medium in presence of thermo-radiation and ohmic viscous dissipation*. Discov. Appl. Sci. 6, 199 (2024). https://doi.org/10.1007/s42452-024-05866-6

32. Ordonez, J. C., Bejan, A., *Entropy generation minimization in parallel-plates counterflow heat exchangers*. Int. J. Energy Res. 24, 843–864 (2000).

33. Ramesh, K., Ojjela, O., *Entropy generation analysis of natural convective radiative second grade nanofluid flow between parallel plates in a porous medium*. Appl. Math. Mech. 40, 481–498 (2019). https://doi.org/10.1007/s10483-019-2464-8

34. Rashidi, S., Akbarzadeh, M., Masoodi, R., Languri, E. M., *Thermal-hydraulic and entropy generation analysis for turbulent flow inside a corrugated channel*. Int. J. Heat Mass Transf. 109, 812–823 (2017). https://doi.org/10.1016/j.ijheatmasstransfer.2017.02.033

35. Shah, Z., Alzahrani, E. O., Alghamdi, W., Ullah, M. Z., *Influences of electrical MHD and Hall current on squeezing nanofluid flow inside rotating porous plates with viscous and Joule dissipation effects*. J. Therm. Anal. Calorim. 140, 1215–1227 (2020). https://doi.org/10.1007/s10973-019-09176-7

36. Sheikhzadeh, G., Aghaei, A., Ehteram, H., Abbaszadeh, M., *Analytical study of parameters affecting entropy generation of nanofluid turbulent flow in channel and micro-channel*. Therm. Sci. 20, 2037–2050 (2016). https://doi.org/10.2298/TSCI151112070S

37. Shojaeian, M., Koşar, A., *Convective heat transfer and entropy generation analysis on Newtonian and non-Newtonian fluid flows between parallel plates under slip boundary conditions*. Int. J. Heat Mass Transf. 70, 664–673 (2014). https://doi.org/10.1016/j.ijheatmasstransfer.2013.11.020

38. Suresh, S., Venkitaraj, K. P., Selvakumar, P., Chandrasekar, M., *Synthesis of Al_2O_3–Cu/water hybrid nanofluids using two-step method and its thermophysical properties*. Colloids Surf. A 388, 41–48 (2011). https://doi.org/10.1016/j.colsurfa.2011.08.005

39. Tsang, Y. W., Tsang, C. F., *Channel model of flow through fractured media*. Water Resour. Res. 23, 467–479 (1987). https://doi.org/10.1029/WR023i003p00467

40. Turkyilmazoglu, M., *MHD fluid flow and heat transfer due to a stretching rotating disk*. Int. J. Therm. Sci. 51, 195–201 (2012). https://doi.org/10.1016/j.ijthermalsci.2011.08.016

41. Upreti, H., Pandey, A. K., Kumar, M., *Unsteady squeezing flow of magnetic hybrid nanofluids within parallel plates and entropy generation*. Heat Transf. 50, 105–125 (2021). https://doi.org/10.1002/htj.21994

42. Xie, Z.-Y., Jian, Y.-J., *Entropy generation of two-layer magnetohydrodynamic electroosmotic flow through microparallel channels*. Energy 139, 1080–1093 (2017). https://doi.org/10.1016/j.energy.2017.08.038

12. Nomenclature

x, y, z	Cartesian coordinates (m)	D_b	Brownian diffusion coefficient (m^2/s)
u, v, w	Velocity components (m/s)	k_2	Chemical reaction rate (1/s)
p	Pressure (N/m^2)	E_a	Activation energy (J/mol)
σ_e	Electric conductivity (S/m)	κ	Boltzmann constant (J/K)
B_0	Magnetic field strength (T)	λ_1	Slip coefficient for velocity (m)
μ	Dynamic viscosity (Pa s)	λ_2	Slip coefficient for temperature (m)
ρ_{hnf}	Density (kg/m^3)	Pr	Prandtl number
$(\rho C_p)_{hnf}$	Specific heat (J/kg K)	Re	Reynolds number
T	Temperature (K)	Mn	Magnetic parameter
C	Concentration (mol/m^3)	Ec	Eckert number
Q_0	Heat generation coefficient (W/m^3)	N	Radiation parameter
k_{nf}	Thermal conductivity (W/mK)	q_r	Heat flux (W/m^2)
k_r	Mean absorption coefficient (1/m)	Le	Lewis number
σ^*	Stefan–Boltzmann constant (W/m^2K^4)	R_0	Rotation parameter
Ω	Angular velocity (rad/s)	θ^*	Temperature
l	Velocity slip parameter	Nu	Nusselt number
l_1	Thermal slip parameter	C_f	Skin friction
β	Temperature ratio	hnf	Hybrid nanofluid
α_0	Chemical reaction rate (1/s)	f	Base fluid

Mandya Seenaiah Pooja,
Department of Mathematics,
School of Applied Sciences, REVA University,
India.
E-mail address: poojasathishkp06@gmail.com

and

Joghaylla Santhosh Kumar,
Department of Mathematics,
School of Applied Sciences, REVA University,
India.
E-mail address: ratnamsanthosh83@gmail.com

and

Kammasandra Munivenkataswamy Praveena Kumara,
Department of Mathematics,
School of Applied Sciences, REVA University,
India.
E-mail address: praveenmsk82@gmail.com

and

Sibyala Vijayakumar Varma,
Department of Mathematics,
School of Applied Sciences, REVA University,
India.
E-mail address: svijayakumarvarma@yahoo.co.in